Mechanics, hydration phase and pore development of embodied energy and carbon composites based on ultrahigh-volume low-carbon cement with

Citation for the original published paper (version of record):
Liu, J., Zhang, W., Li, Z. et al (2022). Mechanics, hydration phase and pore development of embodied energy and carbon composites based
on ultrahigh-volume low-carbon cement with limestone calcined clay. Case Studies in Construction Materials, 17. http://dx.doi.org/10.1016/j.cscm.2022.e01299

(article starts on next page)

Case Studies in Construction Materials 17 (2022) e01299

Contents lists available at ScienceDirect

Case Studies in Construction Materials

journal homepage: www.elsevier.com/locate/cscm

Mechanics, hydration phase and pore development of embodied energy and carbon composites based on ultrahigh-volume low-carbon cement with limestone calcined clay

Jun Liu [a], Weizhuo Zhang [a], Zhenlin Li [a], Hesong Jin [a,*], Luping Tang [b]

[a] Guangdong Provincial Key Laboratory of Durability for Marine Civil Engineering, College of Civil and Transportation Engineering, Shenzhen University, Shenzhen 518060, PR China

[b] Department of Architecture and Civil Engineering, Division of Building Technology, Chalmers University of Technology, 41296 Gothenburg, Sweden

ARTICLE INFO

Keywords:
Engineered cementitious composites
Low-carbon cement with limestone calcined clay
Fluidity
Mechanical properties
Microstructure
Sustainability

ABSTRACT

Engineered cement-based composites exhibit excellent deformability, mechanical behavior, fresh performance and durability. However, the traditional cement-based composites incorporating high volume ordinary Portland cement would lead to high carbon footprint. In this study, a new and eco-efficient engineered cement-based composites was designed by incorporating Polypropylene fibers (PPF) and eco-friendly cement with limestone calcined clay (LC3-ECCs). The LC3-ECCs were analyzed and discussed in terms of mechanical properties, microscopic morphology, hydration products and porosity. The study found that the 28-days compressive behavior was above 44.2 MPa, and the flexural strength remained above 4.8 MPa. Because of the formation and gathering of highly polymerized compound products (C-S-H gel, C-A-S-H gel) in the matrix and plenty of ettringite, the bonding effect between PPF and LC3 cementitious matrix is better. Additionally, the LC3-ECCs with 1.5 % volume content of PP fiber showed less porosity beneficial to the mechanical behavior. This study suggests that low-carbon LC3 has the potential to be successfully utilized as the alternative to OPC and is suitable to design sustainable ECCs, and this low-carbon construction product can be also generally applied into some area with the abundant clay sources.

1. Introduction

As an important cementitious material, Portland cement is widely used in civil infrastructures and transportation systems. With rapid global population growth and increasing urbanization, to meet the development of civil facilities systems, the demanding amount for cement is also rising [1]. However, the production of cement requires the utilization of plenty of natural raw materials. Raw materials not only consume energy in the production process [2], but also emit a lot of carbon dioxide (CO_2) into the aerosphere [3]. Additionally, according to reports or statistics, the CO_2 produced by the producing of cement is the proportion for 5–7 % of the global anthropogenic CO_2 emissions [4]. If CO_2 emissions from ordinary Portland cement (OPC) manufacturing can be effectively lowered, it will make a significant contribution to the world climate and environment.

Recently, there are many solutions to reduce the CO_2 produced by cement. Among them, the utilization of alternatives is the focus

* Corresponding author.
E-mail address: jhs199315@my.swjtu.edu.cn (H. Jin).

https://doi.org/10.1016/j.cscm.2022.e01299
Received 4 May 2022; Received in revised form 28 June 2022; Accepted 4 July 2022
Available online 7 July 2022

Fig. 1. Materials applied in the study.

of researches, mainly including energy recovery, alternative raw materials, alternative fuels and exploration of new clinker components [5]. There have been numerous studies [5–7] on alternative binders, which have been applied into mitigating the impact of the carbon footprint associated with cement production on natural resources. Supplementary cementitious materials (SCMs) not only consume less energy and emit fewer greenhouse gases than cement, but also avoids bonding quality issues [8]. At the same time, it has been verified that concrete using some commonly used SCMs, including silica fume (SF), metakaolin, fly ash (FA), and blast furnace slag, can exhibit better effects than conventional concrete [9–11]. Therefore, among all the alternatives, replacing part of the cement with SCMs is one of the most promising strategies [12]. It has also led to the continuous reducing of the clinker volume in OPC and the increasing replacement of SCMs worldwide [13]. However, the current problem is that most of the widely used SCMs are industrial by-products. It means that both existing reserves and forecasting production will be constrained, limiting the large-scale use of these SCMs. Therefore, the expected demand for complete replacement of cement will not be met [7]. Additionally, the high substitution levels of these materials usually exhibit some problems that are detrimental to the early performance of concrete, such as delayed setting and strength development [14]. Therefore, it is meaningful and valuable to explore a new type of SCM with higher yield and better performance.

To achieve the needs of sustainable manufacturing and applications of OPC, limestone calcined clay (LC2), as a new SCM, has an early mechanical behavior similar to that of OPC. Furthermore, eco-friendly cement with limestone calcined clay (LC3) has been popularized and applied in Cuba and India because it demonstrates similar properties to ordinary Portland cement [15]. LC3 is a low-carbon cement with a ternary binder system composed of limestone and calcined clay [2]. It is a composite cement material with less impact on the environment [16]. Compared with traditional cement, LC3 has a greater competitive advantage. Firstly, the clay in LC3 is abundant in the earth's crust and available across regions [17]. It only needs to be calcined to produce calcined clay [18]. More importantly, LC3 showed a higher level of clinker substitution and maintains the same or better mechanical properties [19], durability [20] and physicochemical properties [21] as conventional cement at high replacement rates. It also means that LC3 is worthy of further study and promotion.

Poor ductility and low tensile strength have always been problems with cement-based materials, which is also reflected in the LC3 system. Until the 1990s, Li et al. combined fibers with cementitious materials to obtain a high-toughness engineering cementitious composite material (ECCs) [22,23]. It demonstrates good mechanical properties, micro crack width, large strain capacity, and self-healing ability. To improve the mechanical properties of LC3, it is necessary to design and study eco-efficient engineering cement-based materials with adding LC3 and fibers (LC3-ECCs). At present, the preliminary exploration of LC3-ECCs has been carried out, and it is investigated that the 28-days compressive behavior achieves the requirements of ordinary structures [24]. Meanwhile, LC3-ECCs exhibit better ductility and durability than OPC-ECCs, as well as low energy consumption and low carbon emissions [25]. It indicates that LC3 shows feasibility in developing sustainable ECCs. However, the hydration of the LC3 matrix and the adhesion of LC3 to fibers under different curing ages of LC3-ECC have not been explored. In addition, the fiber content will affect the mechanical properties and working performance of the material, and it will also cause an increase in cost, which has not been considered in previous studies.

This study explores the mechanical properties of LC3-ECCs under 6 fiber contents and 4 curing ages, including compressive strength and flexural strength. The relationship between fiber content and mechanical properties during curing age was explored. The fluidity of LC3-ECCs was studied and his work performance was evaluated. The micro characteristics of LC3-ECCs are analyzed and investigated by SEM, MIP and TGA. In this study, LC3, a new low-carbon cement, has been preliminarily studied in the field of composite materials. It would provide practical ideas and theoretical insight for the promotion and application of LC3.

Table 1
Chemical characteristics of raw materials (%).

Type of materials	SiO_2	Al_2O_3	CaO	K_2O	Fe_2O_3	MgO	SO_3
C2	55.8	38	0.26	3.35	1.57	0.35	0.18
OPC clinker	20.31	5.62	61.78	1.55	3.54	2.11	2.47

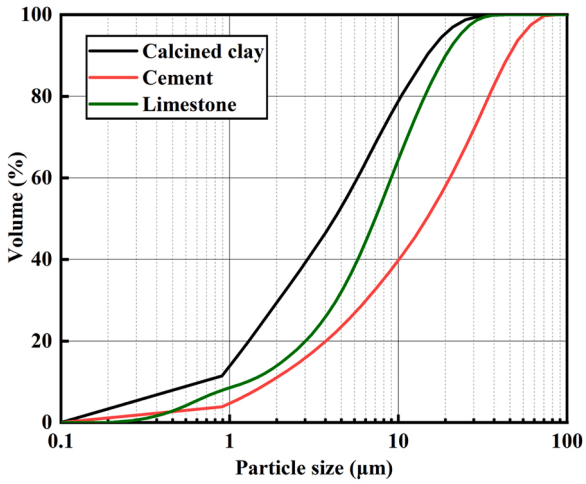

Fig. 2. Particle size analysis of raw materials.

2. Experimental materials and testing methods

2.1. Materials

The raw materials were shown in Fig. 1. In this work, OPC was from a Conch brand product from Yingde City, Guangdong Province. The calcined clay (C2) used in this study was made from kaolin tailings calcined at 700–800 °C collected during an industrial pilot production in Maoming, Guangdong, China. The chemical features of raw materials are listed in Table 1. In addition, limestone consists of $CaCO_3$. Gypsum is composed of analytically pure $CaSO_4{\cdot}2H_2O$, which acts to ease the setting time. Polypropylene (PP) fibers have a length of 1.2 cm, a diameter of 25 μm, a Young's modulus of 7.1 GPa, and a tensile strength of 630 MPa. The particle size analysis of calcined clay and OPC clinker is shown in Fig. 2. The particle size feature is basically maintained at 0.1–100 μm. The rule of PS is: calcined clay < limestone < cement.

Fig. 3 shows the microstructure of the raw material under the SEM. Fig. 3(a)–(d) are limestone, calcined clay, cement and gypsum, respectively, which are the main constituent materials of LC3. The calcined clay particles exhibit random shapes, including massive and flocculent particles. The cement is in the form of irregular granules. In addition, the XRD of limestone, C2 and OPC clinker as shown in Fig. 4(a–c) mainly contain crystalline substances such as calcite, muscovite, quartz, rutile, belite and alite. The main amorphous content of C2 is metakaolin. These substances are beneficial to promote the chemical reaction behavior of LC3.

2.2. Mixture proportions and specimens manufacturing

This study set the water-to-binder ratio (w/b) of ECC to 0.4 referring to previous studies [20]. The contents of limestone, OPC clinker, C2 and gypsum are the usual proportions of LC3, which are 50 %, 30 %, 15 % and 5 % respectively. OPC contains 5 % gypsum, and only needs to add 2.4 % gypsum. This work explored the curing times of 1 d, 3 d, 7 d and 28 d, respectively. Moreover, 6 kinds of fiber content with different volume ratios were designed, which were 0 %, 0.5 %, 1 %, 1.5 %, 2 % and 2.5 %, respectively. The detailed mixture proportions were shown in Table 2. The LC3-F0.0 with 0 % fiber content was the paste, and the other groups were ECCs.

The fabrication of the specimens in line with the requirements of *GB/T 17671-1999* [26]. The specific preparation process of the specimen is shown in Fig. 5. First putting the cementitious material into the mortar mixer for 2 min and mixing evenly, then gradually adding the PP fibers to avoid the fibers winding due to too fast speed, and finally adding water and mixing for 2 min before putting it into the mold. The dimension of the fabricated specimens was 40 mm × 40 mm × 160 mm and there were 3 test samples in each composites group. The samples were demoulded after 1 day and putted in a constant temperature and humidity curing room. In the curing room, the temperature was kept at 20 ± 2 ℃ and the humidity was kept above 95 %.

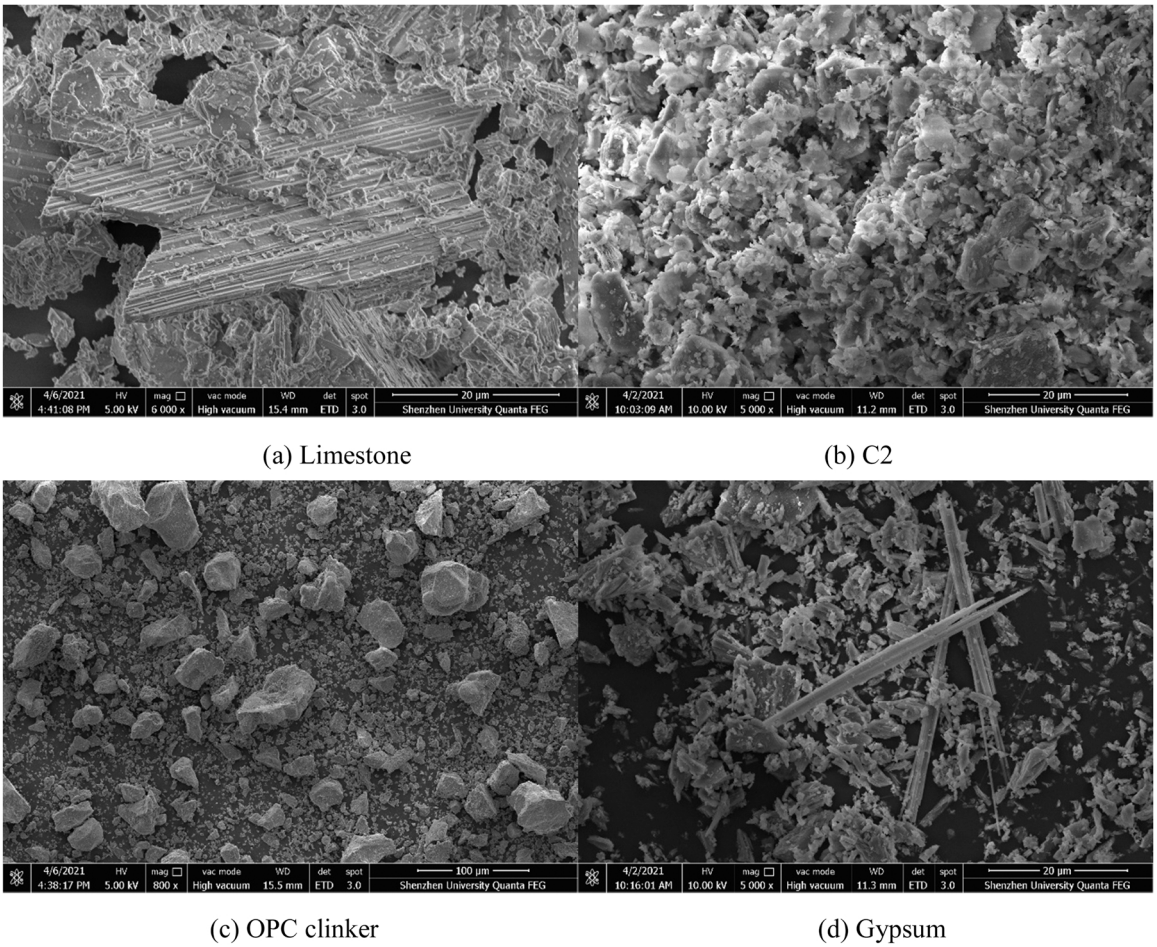

Fig. 3. The microstructure of raw materials.

2.3. Testing program in the research project

2.3.1. The testing procedure of fluidity

Fig. 6 shows the samples on which the tests were performed, as well as the equipment used for each test, including those for fluidity, mechanical properties, SEM-EDS, MIP, XRD and TG/DTG. According to the Chinese specification *GB/T2419-2005* [27], the fluidity of LC3-ECCs was measured using jumping tables, mold trials, tampers and calipers. The fresh paste was placed in the test mold, and after the tamping is completed, the test mold is removed and 25 beats are completed on the jumping table. The width of the expansion of the paste in two vertical directions was recorded to represent the fluidity of the freshly mixed slurry paste. The characteristic deformability factor (Γ) was obtained as:

$$\Gamma = (D_1 - D_0)/D_0 \tag{1}$$

where D_1 is the average of the two readings of diameters after dropping, and D_0 is the diameter of the cone bottom (100 mm).

2.3.2. The testing procedure of compressive and flexural characteristics

The specimens were manufactured according to Section 2.2. They are taken out and used after reaching the designed different curing times. The flexural strength and compressive strength were obtained according to *GB/T 17671-1999* [26]. The testing samples were operated for flexural feature first and the loading speed was set to 50 N/s. Then the compressive strength test of the fractured specimen, half of the specimens tested after flexural test and no crack at their compression section, was carried out. The loading speed was set to 2.5 kN/s.

2.3.3. The testing procedure of SEM-EDS

SEM-EDS was performed on the fracture surface of the specimens which diameter was about 10 mm through compressive failure. They were first prevented from hydration. Afterwards, the experimental blocks were placed in a vacuum drying oven with a

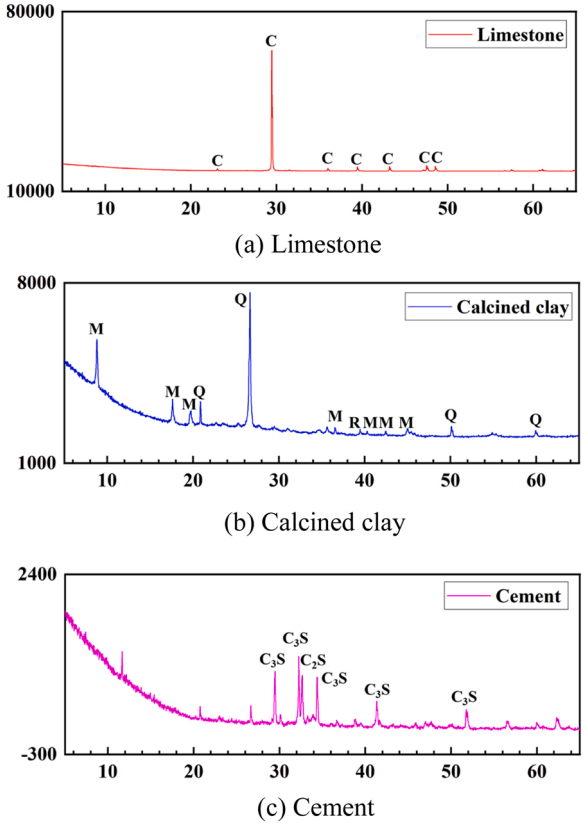

Fig. 4. XRD of raw materials (C: calcite, M: muscovite, Q: quartz, R: rutile, C_2S: belite, C_3S: alite).

Table 2
Mix proportions of LC3-ECCs.

No.	w/b	Binder proportion				PP fiber (vol%)
		OPC clinker	Calcined Clay	Limestone	Gypsum	
LC3-F0.0	0.4	0.5	0.3	0.15	0.05	0
LC3-F0.5	0.4	0.5	0.3	0.15	0.05	0.5
LC3-F1.0	0.4	0.5	0.3	0.15	0.05	1
LC3-F1.5	0.4	0.5	0.3	0.15	0.05	1.5
LC3-F2.0	0.4	0.5	0.3	0.15	0.05	2
LC3-F2.5	0.4	0.5	0.3	0.15	0.05	2.5

Note: F is for PP fiber and the numbers is for PP fibers with volume proportions of 0 %, 0.5 %, 1 %, 1.5 %, 2 %, and 2.5 %, respectively.

temperature set to 60 ℃ for more than 3 days until the sample mass no longer changed. Before SEM test, the surfaces of the experimental samples were sprayed with gold to increase the conductivity. The surfaces of the samples were observed using a SEM-EDS equipment and the machine is Quanta TM 250 FEG field emission environmental SEM-EDS. The working voltage of SEM is 20 kV.

2.3.4. The testing procedure of XRD

The specimens that reached the design curing age were first prevented from hydration for 2 days with absolute ethanol, then ground and sieved by a 200-mesh sieve. The test specimens were analyzed using the D8 X-ray diffractometer produced by Bruker, Germany. The scanning angle is set in the range of 5–65° of 2θ, the testing step size is 0.1 and the scanning time is 0.2 s.

2.3.5. The testing procedure of TG/DTA

Thermogravimetric analysis was conducted and the testing machine is a STA 409PC comprehensive thermal analyzer and the equipment is from Nachi (Shanghai) Co., Ltd. with a temperature range of 30–1000 °C and a heating rate of 10 °C/min. The test was carried out under N_2 atmosphere.

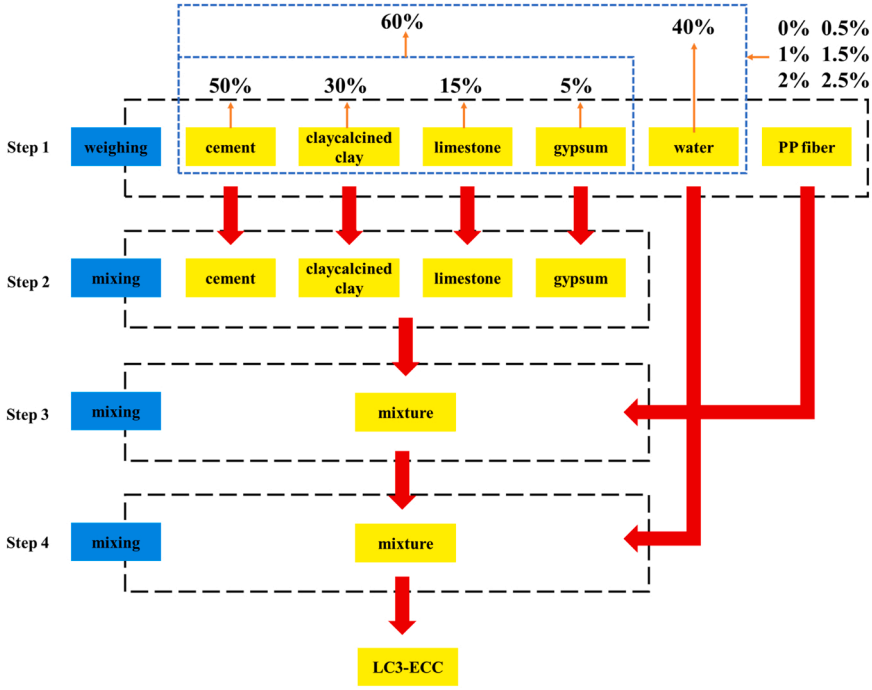

Fig. 5. Specimen preparation process.

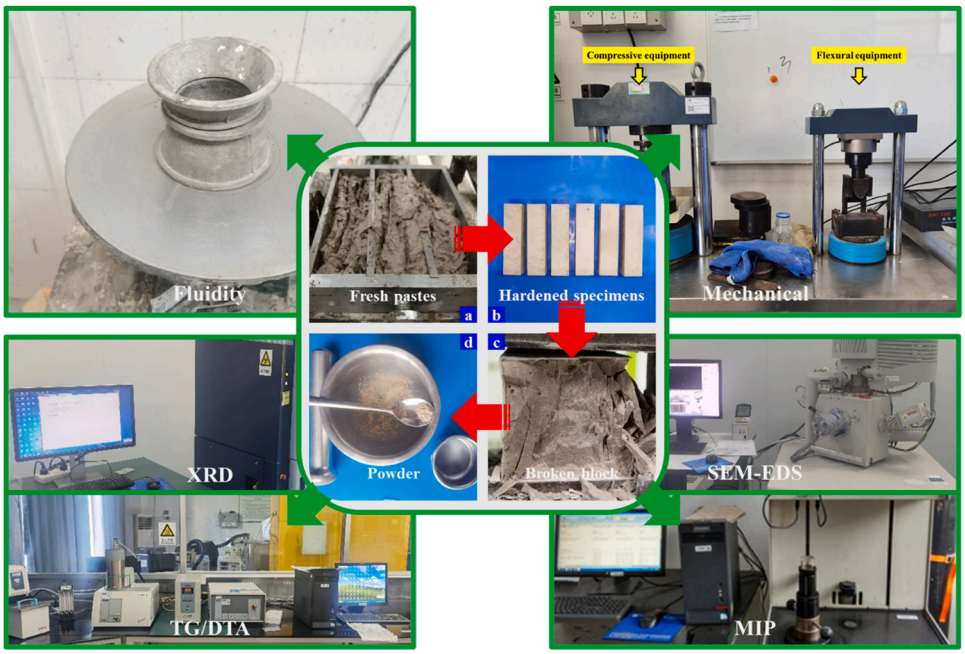

Fig. 6. Test operation process.

2.3.6. The testing procedure of MIP

Small test blocks with side lengths of 10 mm were placed in the vacuum drying oven. MIP testing was operated and the testing equipment is a Micromeritics Autopore IV 9510 mercury porosimeter. The corresponding minimum pore size in the test was about 3 nm.

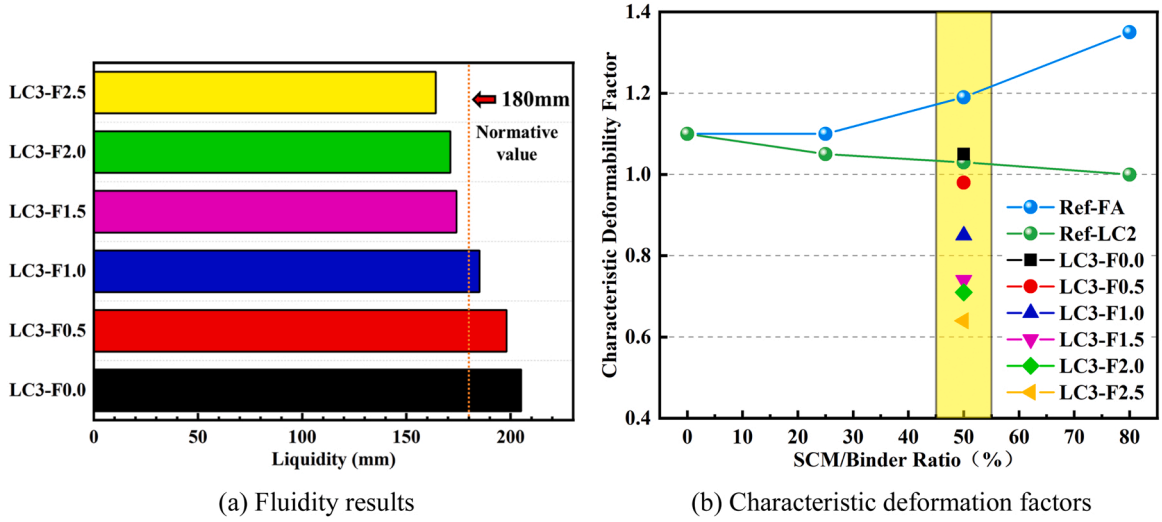

Fig. 7. Fluidity of LC3-ECCs (Ref-FA and Ref-LC2 reference [29]).

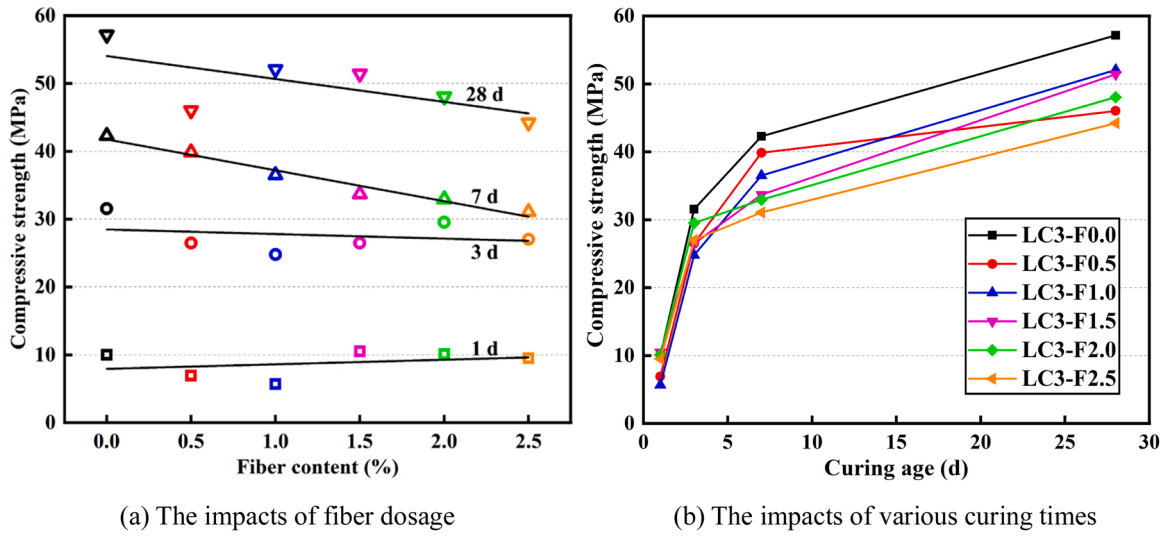

Fig. 8. Compressive strength of LC3-ECCs.

3. Results and discussion

3.1. Fluidity analysis

Fig. 7(a) shows the data of the fluidity test. The fluidity of the freshly mixed pastes of LC3-F0.0 to LC3-F2.5 are 205 mm, 198 mm, 185 mm, 174 mm, 171 mm and 164 mm, respectively. The content of PP fiber will reduce the fluidity of the pastes resulting in the continuous decrease of the development area with the increase of the content of PP fiber. Usually, the ratio at 180 mm fluidity is used as the minimum water consumption of the material. When the fluidity is less than 180 mm, the water-cement ratio is adjusted by an integer multiple of 0.01 to make the fluidity of the mortar not less than 180 mm [28]. The fluidity of LC3-F0.0, LC3-F0.5 and LC3-F1.0 did not meet the requirements of the standard [28], so the water-to-binder ratio can be appropriately increased during preparation to improve their working performance.

Fig. 7(b) shows the characteristic deformation factors of LC3-ECCs and the two control groups Ref-FA and Ref-LC2 in [29]. The flow characteristic coefficient of Ref-FA increases with the increase of SCMs content, while the flow characteristic coefficient of Ref-LC2 decreases with the increase of SCMs content. Due to the larger fineness and specific surface area of calcined clays [30], calcined clays can adsorb more water than fly ash [31], exhibiting poorer fluidity relative to other SCMs. Calcined clay usually increases the water demand of the material [32], while limestone can reduce the water consumption [31], so in LC3 system, calcined clay and

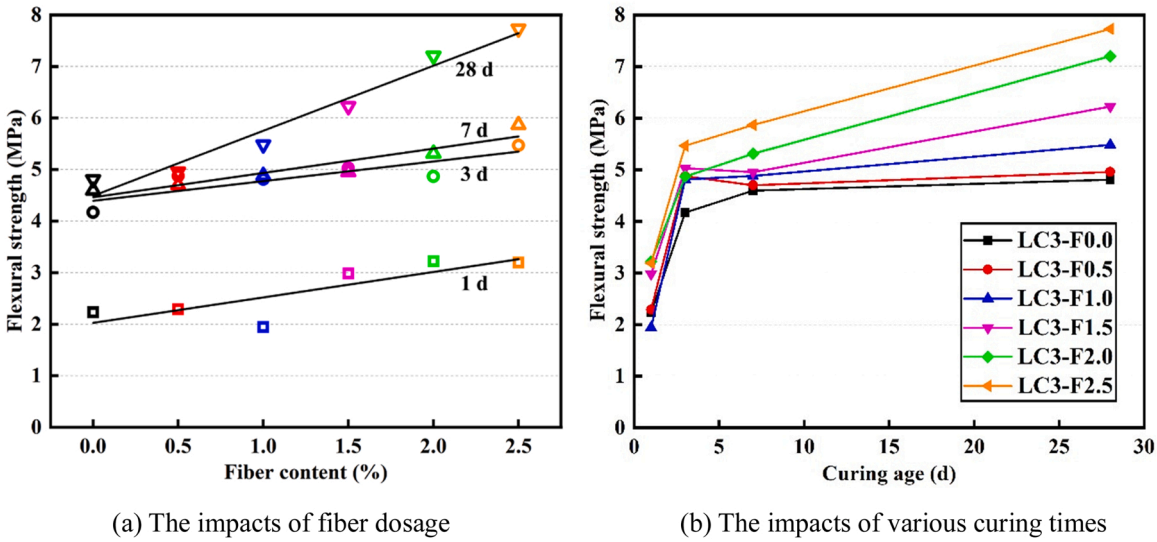

(a) The impacts of fiber dosage (b) The impacts of various curing times

Fig. 9. Flexural strength of LC3-ECCs.

limestone are usually mixed in a ratio of 2:1. This can not only promote the mutual hydration reaction, but also adjust the water consumption of the cement and improve the working performance of the material. The fluidity of LC3-ECCs was inhibited by both clay minerals and PP fibers, but still met the working requirements under the condition of 50% SCMs replacement rate and 1 % volume content of PP fibers.

3.2. Strength development

3.2.1. Compressive

Fig. 8(a–b) show the effects of PPFs volume and curing age on the compressive features of LC3-ECCs, respectively. The 28-days compressive strength (CS) of the 6 groups of samples increase to 57.1 MPa, 46.0 MPa, 52.1 MPa, 51.4 MPa, 48.0 MPa and 44.2 MPa, respectively. During the curing process from 3 d to 7 d, the CS of LC3-F2.0 and LC3-F2.5 increase slightly, what are only 3.4 MPa and 4.0 MPa, respectively. During the curing process from 7 d to 28 d, the CS of LC3-F0.5 increases the smallest, what is only 6.2 MPa.

Research [33] found that ECCs would introduce at the same time with the addition of fibers and the rising of fiber content will usually result in the ascent of air content in the gel matrix. This phenomenon is also further discussed in the research [34] that the compressive strength rising with decreasing fiber volume. However, in this studying project, the relationship between PPFs and CS do not show regularity at 1 d and 3 d. It may be because at early age, the fiber reduces the compressive strength by introducing pores, and the bonding effects between the PPFs and composites matrix enhances the compressive strength. When the curing age was 7-days and 28-days, CS decrease with the increase of the amount of PPFs. The 7-days and 28-days CS of LC3-F2.5 to LC3-F0.0 decreased from 42.3 MPa to 31.1 MPa and 57.1 MPa to 44.2 MPa, respectively. It is worth noting that LC3-F0.5 does not conform to the law at the 28 d. It can be found that LC3-F0.5 has the smallest increase in compressive strength from 7 d to 28 d, which is only 6.2 MPa. It may be because the transverse deformation and failure of the matrix cannot be effectively restrained during the compressive process when the fiber volume content is less than 0.5 %, resulting in the low **CS** of LC3-F0.5.

3.2.2. Flexural

Fig. 9(a–b) are the effects of fiber dosage and various curing times on the flexural characteristics of LC3-ECCs, respectively. The 1 d flexural strength (FS) of the 6 groups of samples are 2.2 MPa, 2.3 MPa, 1.9 MPa, 3.0 MPa, 3.2 MPa and 3.2 MPa, respectively. It is worth noting that the LC3-ECCs increased only a small amount of flexural strength during the curing process from 3 d to 7 d. The 28-days flexural strength of 6 groups increases to 4.8 MPa, 5.0 MPa, 5.5 MPa, 6.2 MPa, 7.2 MPa and 7.7 MPa, respectively.

During the curing process from 7 d to 28 d, the FS growth rate of LC3-ECCs showed an obvious trend. With the ascent of fiber dosage, the increment of flexural strength is also increasing. The increase ranges from LC3-F0.0 to LC3-F2.5 is from 0.2 MPa to 1.9 MPa. Surprisingly, the flexural strength of LC3-F0.0 and LC3-F0.5 is basically unchanged. It shows that LC3-F0.0 has basically reached the final flexural strength at the 3 d, while the strengths of other groups continue to increase during the 28-days curing process. The 28-days flexural strength of LC3-ECCs increase continuously with the increasing of fiber dosage, which is the same with [34]. After the fiber is introduced into the LC3, the fiber acts as a bridge to the matrix, resulting in increased flexural strength. At the same time, the fiber toughening effect is proportional to the fiber content within a certain range, so the FS of the composites increases with the increasing of the PPFs dosage.

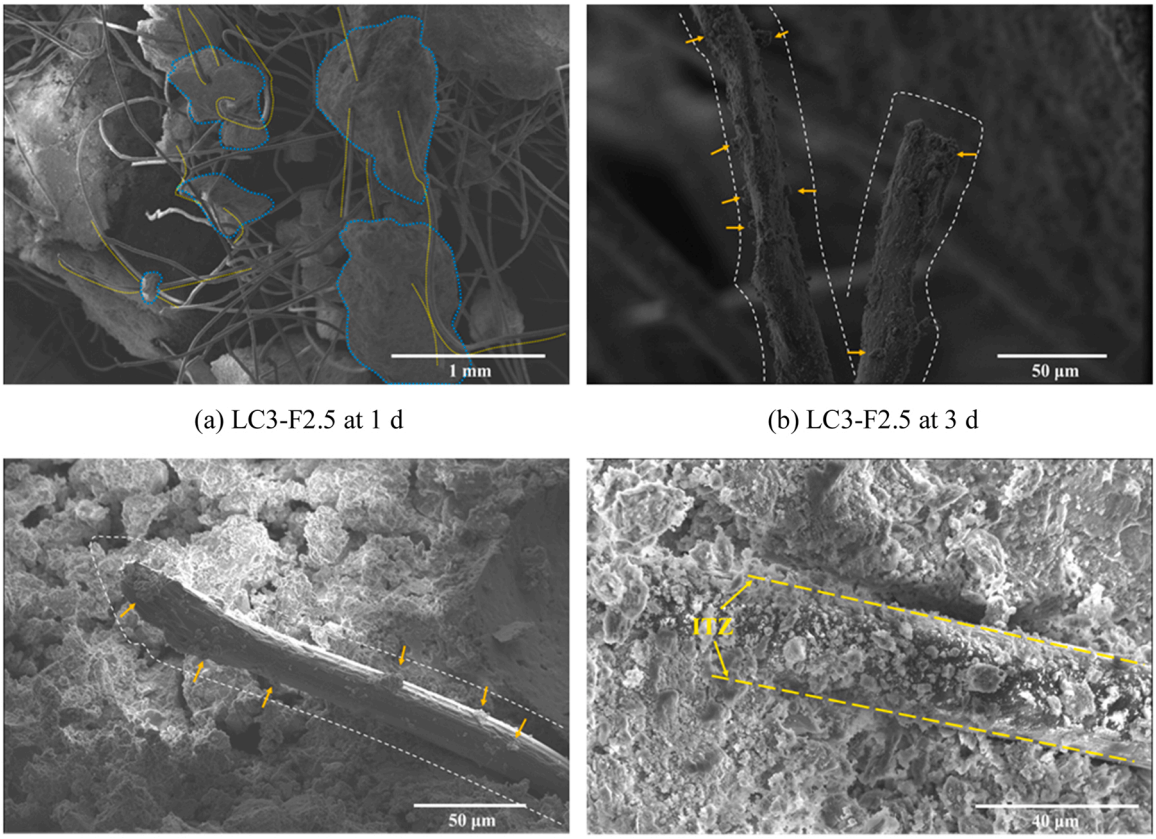

(a) LC3-F2.5 at 1 d (b) LC3-F2.5 at 3 d

(c) LC3-F2.5 at 7 d (d) LC3-F2.5 at 28 d

Fig. 10. Microstructure between PP fibers and LC3 matrix in LC3-ECCs.

3.3. Micromorphology analysis using SEM-EDS

Fig. 10(a) shows the microscopic morphology of LC3-F2.5 after failure at a magnification of 110 times and a curing time of 1 d. It can be observed that the PP fiber and the cement-based matrix are damaged and separated under the impact of compressive load. However, due to the PP fibers, the damaged matrix is connected and the mass loss of the specimen is reduced. The PP fibers act as crack bridges at cracks, increasing the material's flexural resistance. The LC3-F0.0 shatters more severely when it is damaged by compression. Fig. 10(b–c) show the microstructure of LC3-F2.5 when the magnification of electron microscope is 1600 × and the testing age is 72 h and 168 h, respectively. The PP fibers in Fig. 10(b) were originally cylindrical, but were deformed due to drawing. In the study [35], it was also observed that the surface of the fibers became rough under stress, resulting in higher frictional stress. Fig. 10 (d) shows the interface transition zones (ITZs) between PPFs and matrix. The bonding behavior between the PP fibers and the composite matrix is relatively tight. However, at high fiber content, more pores appear. Pores at the ITZ are further analyzed in the Section 3.6.

Fig. 11 shows the microscopic products under SEM analysis at four curing ages with magnifications ranging from 6000 × to 50,000 ×. The main products of LC3 hydration reaction are C-(A)-S-H, CH, AFt, AFm, limestone particles, quartz and feldspar et al. [36]. These species can be observed in Fig. 11. In addition, pores and the looser appearance can be observed in the LC3 matrix. For the samples at the 1 d curing age, unhydrated material and hydrating material can be observed, producing a lot of flocculent C-S-H gels and needle-like AFt. At the beginning of hydration reaction, the contents of sulfate and silicate are high, what results in AFt become the hydration product of crystallization. At 3 d curing age, the C-(A)-S-H gel is already very dense and AFt also begins to change from needle-like to rod-like. C-(A)-S-H gel wraps AFt into interlocking structure. It is explained in the literature [37] that the reaction of LC2 and CH will react to form more C-A-S-H gel, and these can be observed during 3 d curing age. When sulfate is exhausted, Aft gel becomes unstable and gradually converts to AFm [38]. However, the forming of AFm not only meets specific chemical conditions, but also needs to meet certain physical conditions. Reference [21] pointed out that the lack of sufficiently large pores will inhibit the growth of the AFm phase. It can also be found by SEM experiment that the flake hexagonal AFm phase is usually formed in cracks, defects and pores, which can be observed in Fig. 11(d).

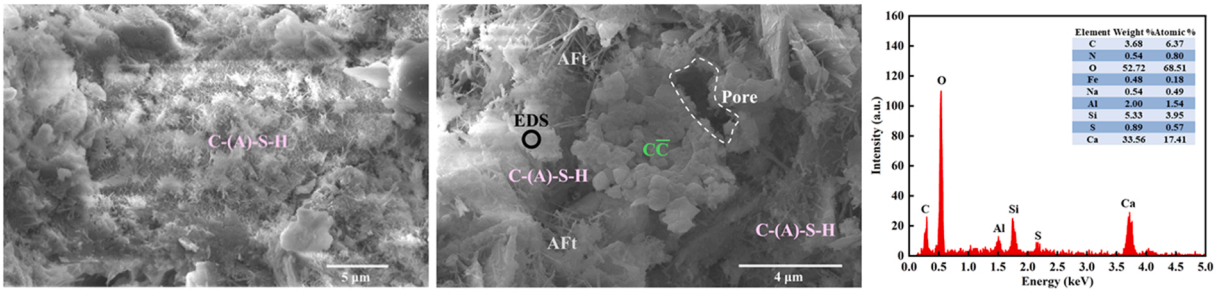

(a) LC3-F0.0 at 1-days

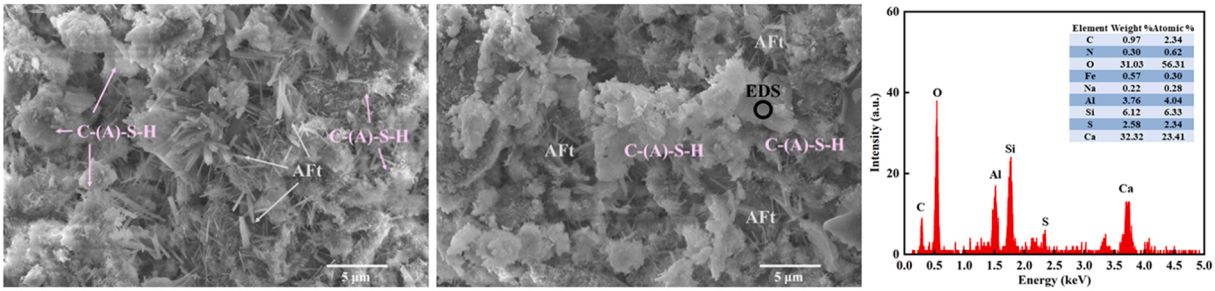

(b) LC3-F0.0 at 3-days

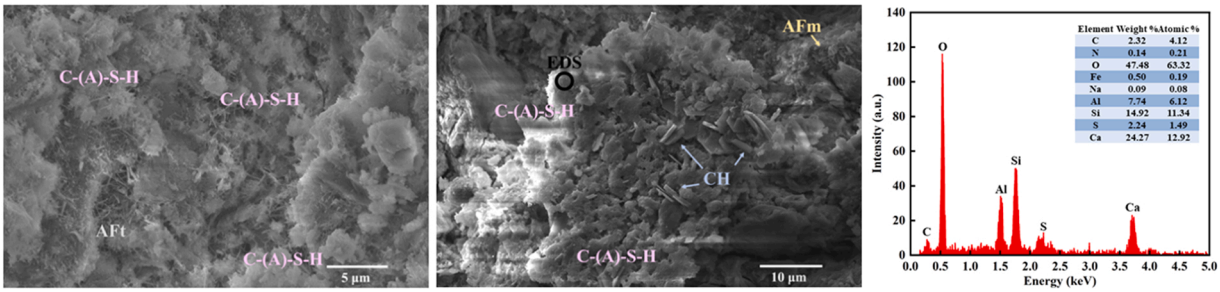

(c) LC3-F0.0 at 7-days

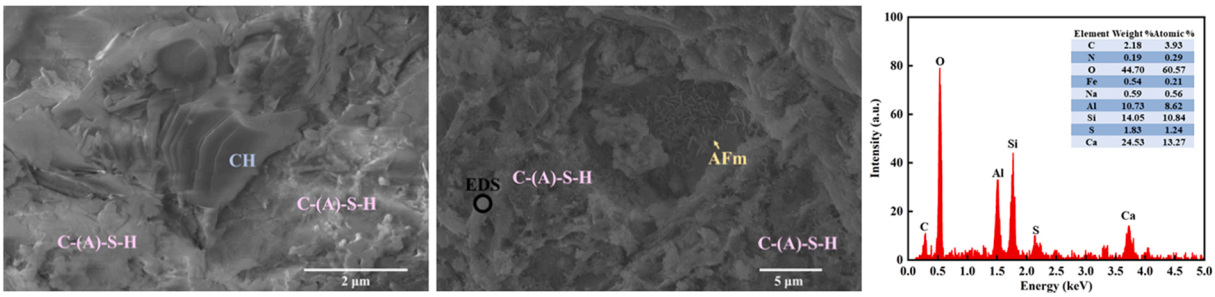

(d) LC3-F0.0 at 28-days

Fig. 11. Microscopic matter and morphology in LC3-ECCs.

3.4. Hydration phase analysis

Fig. 12 respectively shows the compounds phase test results. The peaks in the compounds phase pattern reflect the generation and consumption of crystals in LC3 with the various curing times, mainly including C$\overline{C}$, CH, E, S, Hc and Mc, *etc.* Since CH and C$\overline{C}$ are necessary for the formation of C-A-S-H compounds and carboaluminate, CH reacts with C$\overline{C}$ products and metakaolin to form C-A-S-H

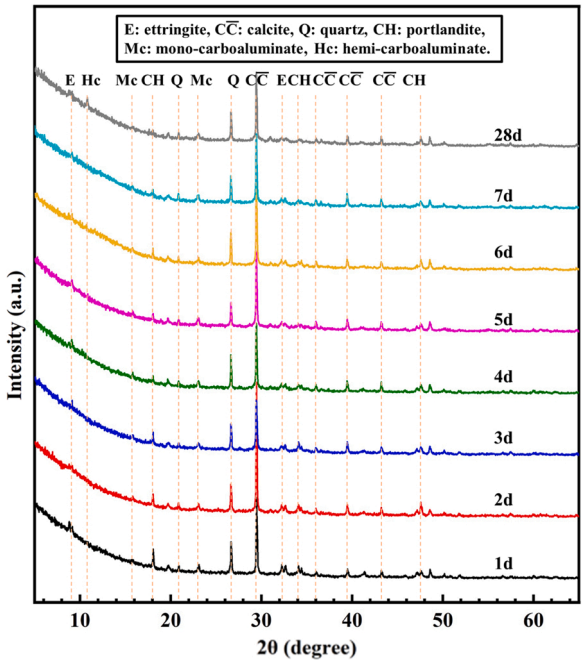

Fig. 12. XRD analysis results of LC3-ECCs.

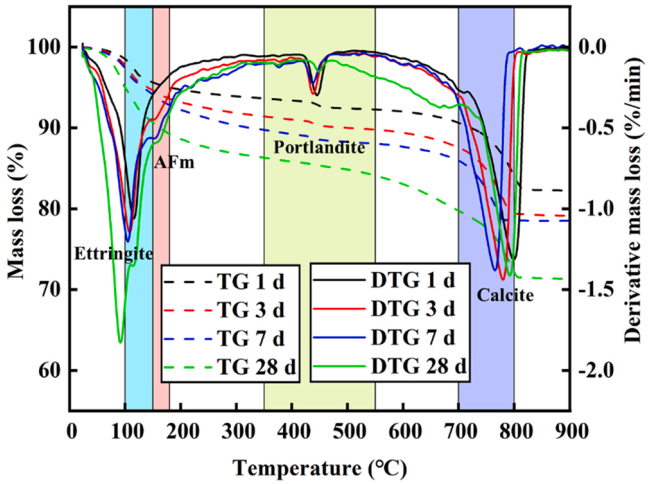

Fig. 13. TG/DTG curves of LC3-ECCs.

gels and carboaluminate [39]. Therefore, compounds of CH and CC̄ are continuously decreasing with the increase of the age. CH also undergoes secondary hydration [17], so CH is consumed. In Fig. 12, CH decreases correspondingly with the increase of the age. The limestone would enhance the forming or producing of Hc and Mc phases. Limestone reacts with activated alumina and calcined clay in C3A to produce Hc and Mc [40]. These carbonoaluminates can promote the mechanical properties of LC3 materials [41]. XRD analysis showed the Hc and Mc, what is different from the data investigated in the study [21]. In this study, Mc had already begun to form at the 1 d curing age, while Hc was formed later. This is more conducive to the producing of Hc rather than Mc [42]. The aluminate phase would react with gypsum to enhance the forming of E. If the aluminate is completely consumed before the gypsum is completely consumed, then more E will continue to be produced [39].

3.5. Thermogravimetry and differential thermal analysis

Fig. 13 reflects the TG/DTG data of LC3-ECCs. The peaks of DTG mainly include ettringite, AFm, portlandite and calcite and their contents correspond to the integrated heat loss of 100–150 ℃, 150–180 ℃, 350–550 ℃ and 700–800 ℃, respectively. Aluminates in

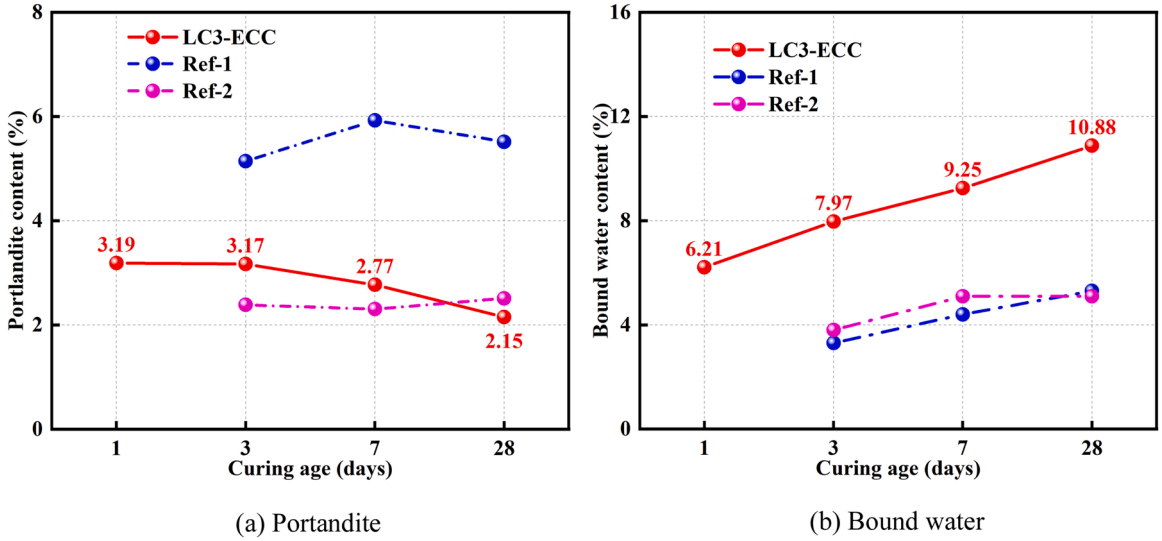

Fig. 14. Changes in product content of TG/DTG test of LC3-ECCs.

clinker contains C_3A and C_4AF. Ettringite is mainly formed by the chemical reaction impacts of gypsum and aluminates [39]. In Fig. 13, ettringite increased with the growth of the curing age and still generated before reaching the 28-days curing conditions. The rephrase of AFm phase increased with the increasing of solidification times and the growth rate slowed down from 7 d to 28 d. This is because of the continuous reducing of the critical pore size during the curing process (Fig. 15) and the lack of sufficiently macro pores inhibits the generating of these AFm phases. It is also discussed in [21] that once the limit of the critical entry radius is reached, the reaction of metakaolin no longer generates the AFm phase. Limestone provides calcite which is produced at short curing times and consumed in subsequent reactions.

Fig. 14(a) shows that the content changes of portlandite are quantified. At 1-day, 3-days, 7-days and 28-days curing conditions, it reached 3.19 %, 3.17 %, 2.77 % and 2.15 %, respectively, and the portlandite content decreased continuously in the later stage of curing. Usually, portlandite as a reaction product will continue to increase with the curing process. It is formed by the chemical reaction influence of C_3S and C_2S in the OPC clinker with free water. But in LC3 system, portlandite is necessary for LC3 pozzolanic reaction [39]. On the one hand, portlandite will react with substances such as AS_2 and be consumed. On the other hand, the reaction of C_2S and AS_2 will produce portlandite. Meanwhile, the portlandite content of Ref-1 is much higher than that of LC3-ECCs and Ref-2. It may be due to the low content of clinker in the LC3 cementitious material, resulting in the competing pozzolanic reaction between metakaolin and FA [43].

Fig. 14(b) exhibits that the content changes of bound water are quantified. At 1-day, 3-days, 7-days and 28-days curing environment, it reached 6.21 %, 7.97 %, 9.25 % and 10.88 %, respectively. The bound water increased during the curing times from 1 d to 7 d and, then remained basically the same during the curing times from 7 d to 28 d. The bound water can reflect the hydrating degree of SCMs. And the bound water of LC3-ECCs in this project is higher than that of Ref-1 and Ref-2 in the study [43].

3.6. Pore analysis

Fig. 15 shows the results of MIP analysis of LC3-ECCs under 3-days and 28-days curing environment, including cumulative pore volume (**CPV**), pore size distribution (**PSD**) and pore volume percentage (**PVP**). In Fig. 15(a) shows under 3-days curing system, with the more fiber content, the more is CPV. Fig. 15(b) shows that the same observation is also present when the curing age is 28 d. Except LC3-F1.5 shows a different phenomenon, others exhibit lower CPV than LC3-F0.0. In the 3-days curing age, the difference in CPV between the groups is small. The difference between LC3-F0.0 with the smallest CPV (= 0.25 mL/g) and LC3-F2.5 with the largest CPV (= 0.29 mL/g) is only 0.04 mL/g. However, in the 28-days curing age, the CPV difference between the groups is larger. The difference between LC3-F1.5 with the smallest CPV (= 0.15 mL/g) and LC3-F2.5 with the largest CPV (0.27 mL/g) is 0.12 mL/g. It shows that the influence of fiber content on porosity is more obvious at long-term curing age.

Fig. 15(c–d) are the PSD of LC3-ECCs at 3-days and 28-days solidification conditions, respectively. At 3 d, the peak of the pores is in the range of 0.01–1 μm. At 28 d, the pores are filled with hydration products, resulting in smaller pore sizes that basically remained below 0.1 μm. According to research [44], adding 2 % volume of PVA fibers will lead to an increase of more than 3 % in the content of pores larger than 0.3 μm. In Fig. 15(d), it can be found that there is a clear peak between 0.1 μm and 1 μm. The peak of LC3-F0.0 in this interval is close to 0.1 μm, while the peak of LC3-F2.5 is larger and the peak of LC3-F2.5 is increased to 0.1 mL/g. The pores can be considered to be generated by the ITZs between the matrix and the PPFs. The pore size is close to 0.2 μm, which can also be reflected in Fig. 10(d). The pore of LC3-F0.0 to LC3-F1.0 do not change significantly. It is worth noting that LC3-F1.5 does not show interfacial pores.

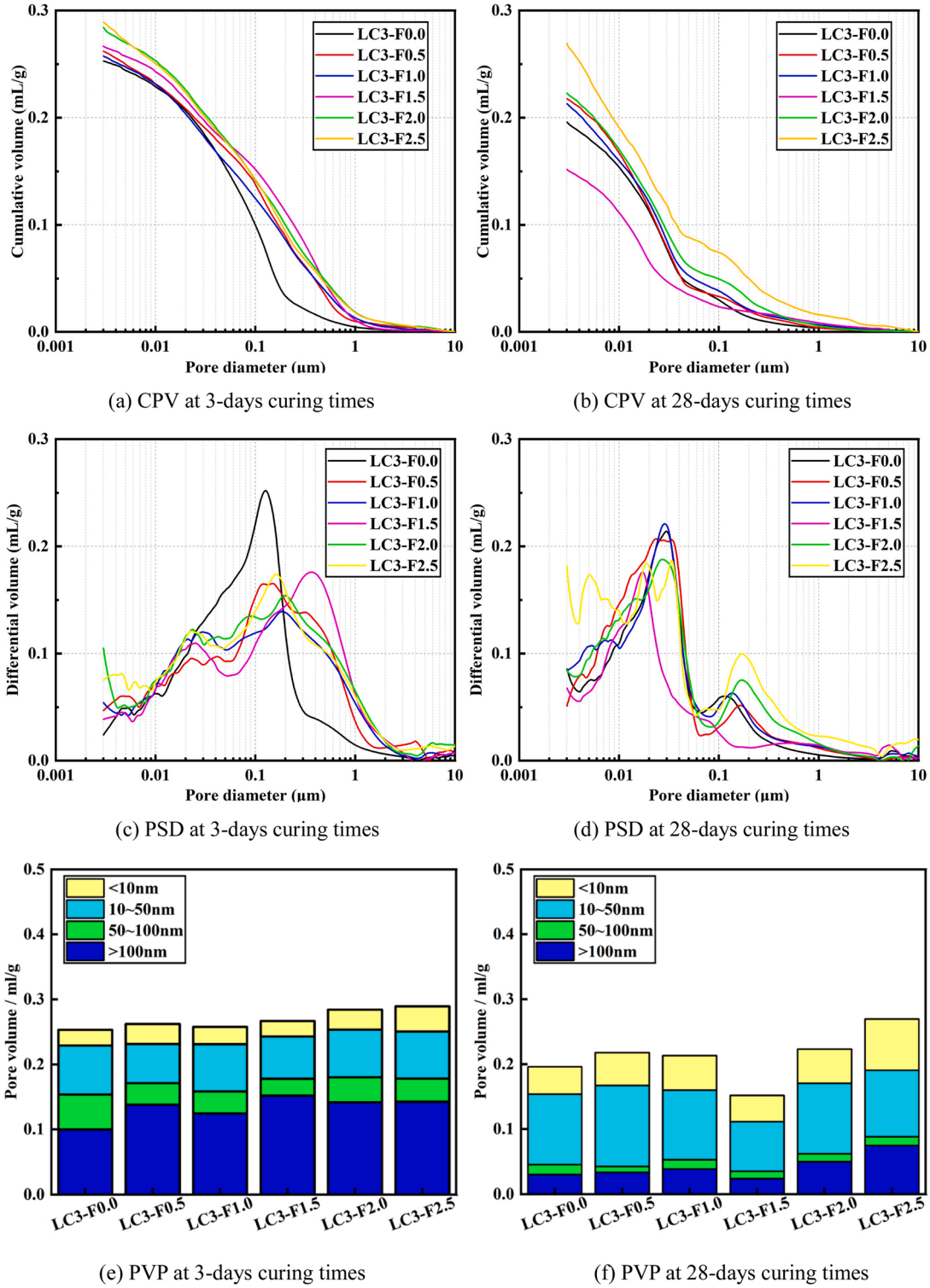

Fig. 15. Pore analysis of LC3-ECCs.

If the pores are divided by function, there will be macro pores (> 100 nm), large capillary pores (50–100 nm), medium capillary pores (10–50 nm) and micro capillary pores (< 10 nm) [45]. Fig. 15(e–f) show the pore volume at 3-days and 28-days curing systems, respectively. The pore size is decreasing from 0.25–0.29 mL/g to 0.15–0.27 mL/g during the hydration process. Simultaneously, the rate of reduction of harmful pores is faster and the amount of macro pores in the pores is also smaller. Macro pores and mesopores are

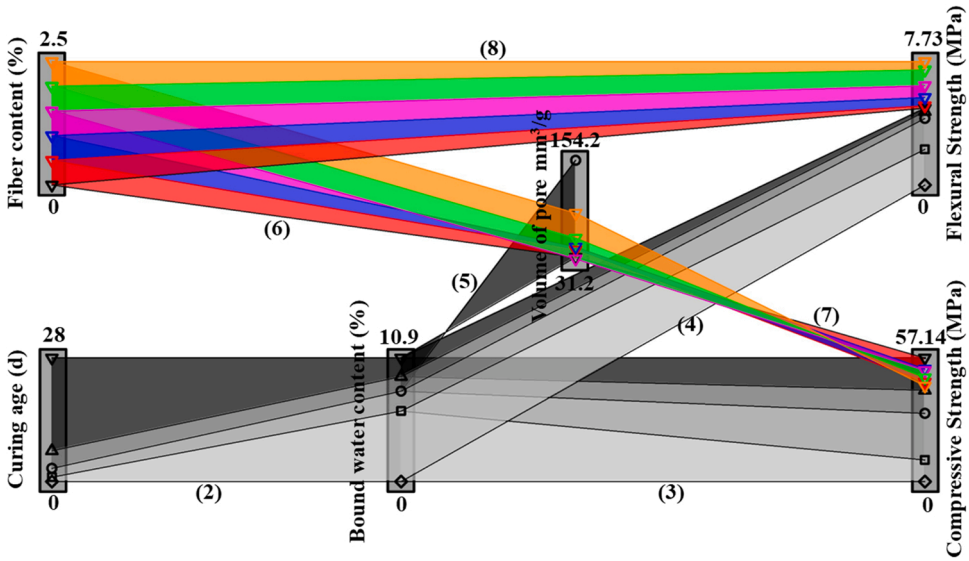

Fig. 16. Relationship between influencing factors of LC-PP-ECCs.

Table 3
Relational equations of influencing factors of LC-PP-ECCs.

Number	Independent variable	Dependent variable	Equation	R^2
(2)	c	ω	$\omega = -5.509e^{-0.190c} + 10.868$	0.98
(3)	ω	f_{cu}	$f_{cu} = 9.991\omega - 50.454$	0.99
(4)	ω	f_{cf}	$f_{cf} = 0.586\omega - 1.126$	0.83
(5)	ω	V_p	$V_p = -25.901\omega + 315.101$	1.00
(6)	V_f	V_p	$V_p = 17.400V_f$	0.59
(7)	V_p	f_{cu}	$f_{cu} = -0.162V_p$	0.41
(8)	V_f	f_{cf}	$f_{cf} = 1.262V_f$	0.96

harmful pores that reduce the mechanical properties and durability of materials [46]. Therefore, comparing the porosity and compressive strength, it can be found that fibers will lead to the increase of total porosity, what in turn will lead to the decrease of the mechanical strength of ECCs.

3.7. The combined effect of fiber content and curing ages on strength

A correlation-based approach is explored here to explore the relationship between compressive and flexural strength with curing age and fiber content. The relationship between curing age (***c***), fiber content (***V_f***), porosity (***V_p***), hydration (***ω***), compressive strength (***f_cu***) and flexural strength (***f_cf***) will be discussed. Under the change of curing ages, the hydration products of cement-based materials continue to increase, resulting in an increase in both compressive strength and flexural strength. The increase of hydration products will also fill the pores. However, the increase of fiber content will increase the porosity. The reduction of macro pores and mesopores in turn leads to improved mechanical properties of the material. Fiber content directly enhances the flexural strength. Therefore, 7 sets of relationships were analyzed, including curing age and bound water content, bound water content and compressive strength, bound water content and flexural strength, bound water content and porosity of macropores, fiber content and macropore porosity, macropore porosity and compressive strength, and fiber content and flexural strength. Fig. 16 shows the influence of fiber content and curing age on the compressive strength and flexural strength of LC3-ECCs. Table 3 is the fitting formula between each relationship. The Eqs. (9)–(10) of the compressive strength can be obtained from Eqs. (2)–(8).

$$f_{cu} = -55.04e^{-0.19c} - (0.05c + 1.42)V_f + 58.13 \tag{9}$$

$$f_{cf} = -3.23e^{-0.19c} + (0.03c + 0.34)V_f + 5.24 \tag{10}$$

Where $\boldsymbol{f_{cu}}$ is the compressive strength, $\boldsymbol{f_{cf}}$ is the compressive strength, $\boldsymbol{c}$ is the curing age, and $\boldsymbol{V_f}$ is the fiber content. Fig. 17(a) is the comparison of Eq. (9) and the measurement results of compressive strength. Fig. 17(b) is the comparison of Eq. (10) and the measurement results of flexural strength. It can be found that there is a good degree of coincidence between the formula and the measured value.

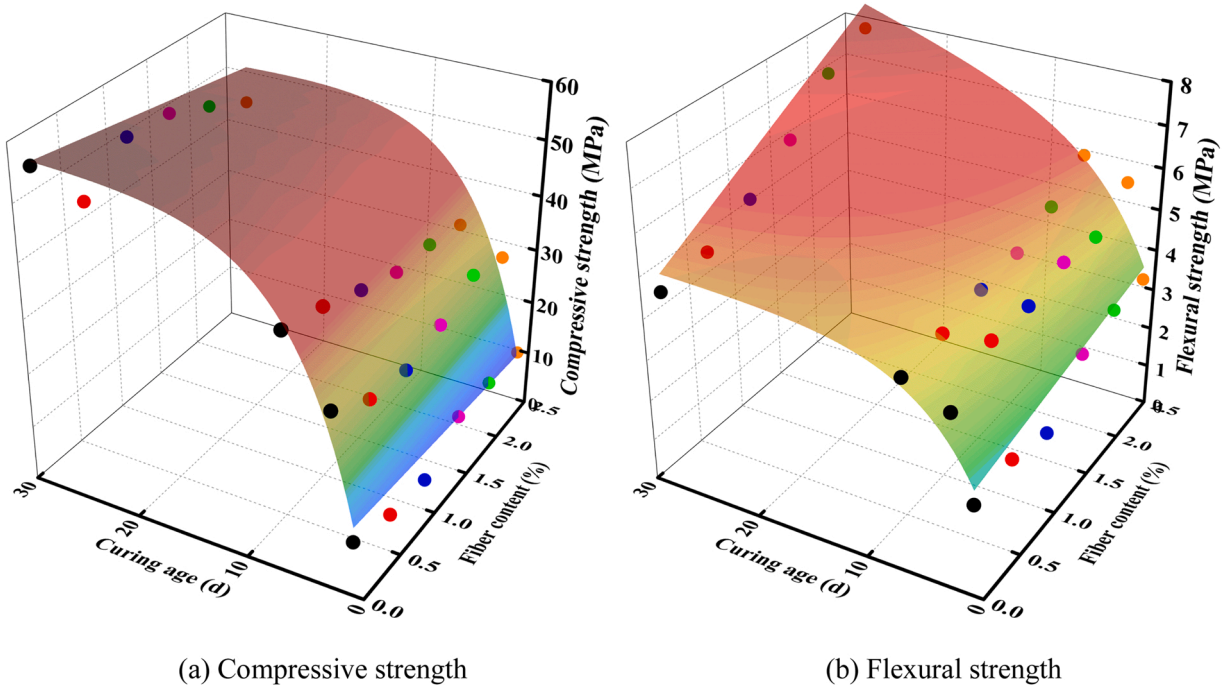

Fig. 17. The results under the influence of fiber content and curing age.

Table 4
Embodied energy, carbon footprint and material cost of the composition of LC3-ECCs.

Mixture	Energy (GJ/t)	CO_2 emission (kg/t)	Cost (USD/t)
LC3	3.99[ab]	550[c]	56.41[c]
PP fiber	77.24[d]	3100[e]	6335[f]
Water	0[g]	0[g]	1.5[g]

[a] Data from [53].
[b] Data from [54].
[c] Data from [16].
[d] Data from [52].
[e] Data from [55].
[f] Data from [56].
[g] Data from [25].

3.8. Environmental and economic assessment

Table 4 lists the material sustainability indicators (MSIs) required to produce LC3-ECCs including energy consumption, CO_2 emissions and cost. The MSIs capture material manufacturing phase at a cradle-to-gate basis and are able to reflect the composite sustainability performance [43]. Some studies [25,43,47–51] are referenced, including various ECCs, ECCs with ultrahigh-volume LC2 matrix, strain hardening cementitious composites (SHCC) with different volume contents of fibers and various concretes. Fig. 18(a) shows the energy consumption of each group. The energy consumption of LC3-ECCs increase from 4 GJ/m^3 to 5.654 GJ/m^3 with the increase of fiber content. Fig. 18(b) shows the CO_2 emission of each group. The CO_2 emission of LC3-ECCs increase from 267.07 kg/m^3 to 339.69 kg/m^3 with the increase of fiber content. Fig. 18(c) shows the cost of each group. The cost of LC3-ECCs increase from 74.95 USD/m^3 to 217.19 USD/m^3. Fig. 18(d) shows the compressive strength of each group. The compressive strength of LC3-ECCs decrease from 57.14 MPa to 44.22 MPa.

Fig. 19 shows MSIs pre unit strength of LC3-ECCs. LC3-F0.0 contributes the smallest embodied energy and embodied carbon per unit compressive strength, which are 0.07 MJ/m^3 MPa and 4.83 kg/m^3 MPa, respectively. LC3-F0.5 contributes the largest embodied energy and embodied carbon per unit flexural strength, which are 0.87 MJ/m^3 MPa and 58.23 kg/m^3 MPa, respectively. The reason that LC3-F0.5 is larger than LC3-F0.0 is that the increase in flexural strength is smaller after the introduction of 0.5 % PP fibers. LC3-F2.5 contributes the largest embodied energy and embodied carbon per unit compressive strength, and on the contrary contributed the smallest embodied energy and embodied carbon per unit flexural strength. Due to the price of PP fiber, with the increase of fiber content, the embodied cost required for unit compressive strength and unit flexural strength continues to increase, that of LC3-F2.5 is

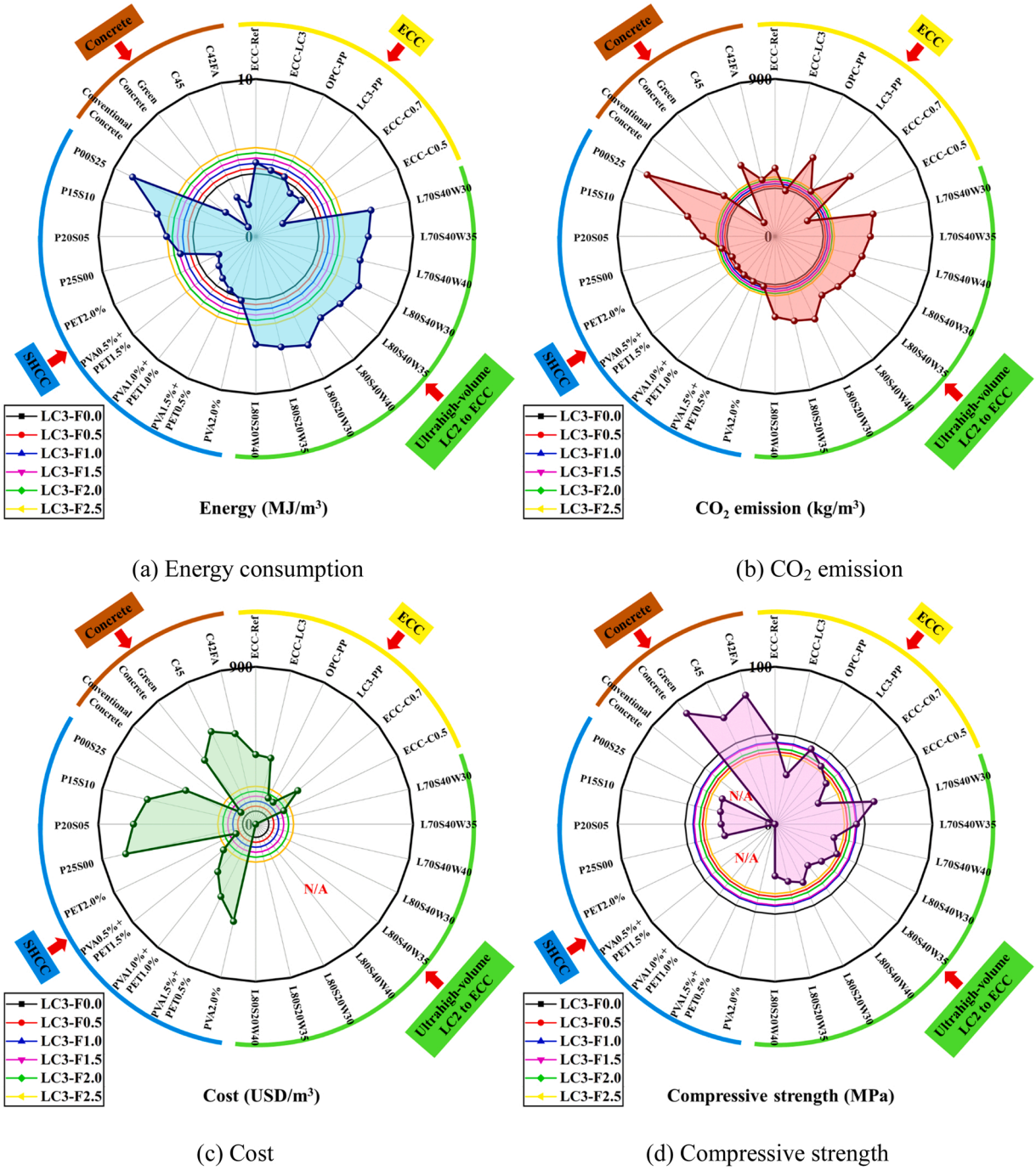

Fig. 18. MSIs between LC3-ECCs and multiple reference materials.

4.91 USD/m^3·MPa and 28.10 USD/m^3 MPa, respectively.

In summary, the advantages and disadvantages of various materials are combined and compared. The energy consumption and CO_2 emission are less affected by the content of PP fiber, while the cost is greatly affected by the content of PP fiber. The study [43] also pointed out that the unit cost of the fiber is higher and the PP fiber used in this study has a greater price advantage than the PVA fiber. The price of PP fiber is usually 6335 USD/t [52] and the price of PVA fiber is usually 12,670 USD/t [51]. The use of cheaper PP fibers is beneficial for sustainable development leading to wider adoption of LC3-ECCs. PP fibers also show better performance than other fibers in compressive strength, but the use of LC3 to make sustainable ECCs still requires more exploration.

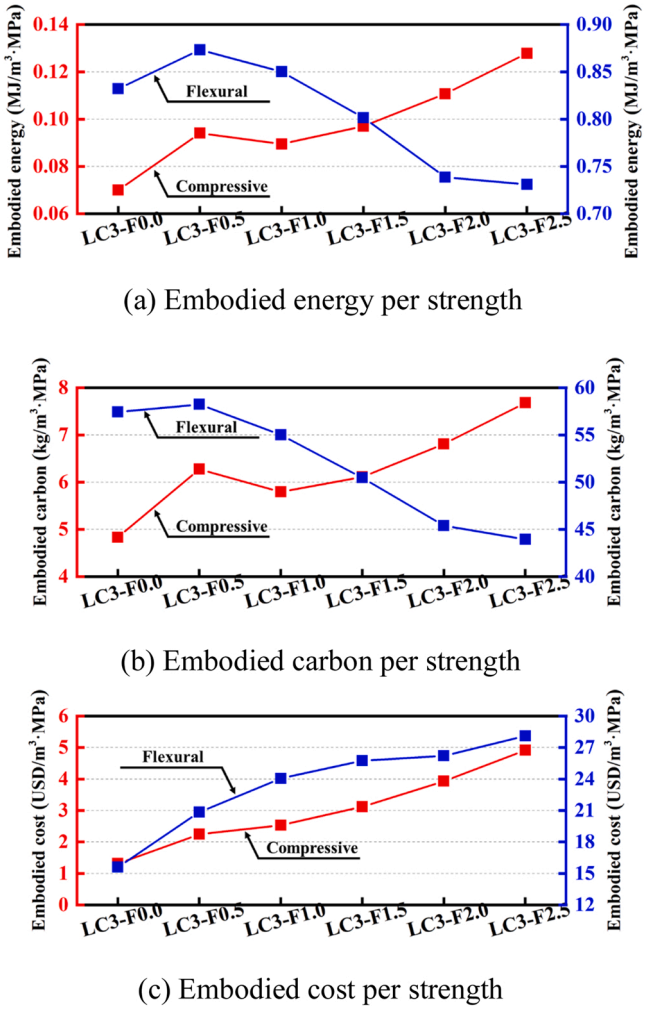

Fig. 19. MSIs per unit strength of LC3-ECCs.

4. Conclusions

In this work, the PP fiber reinforced LC3 matrix was studied under the conditions of 6 fiber contents (0 %, 0.5 %, 1 %, 1.5 %, 2 % and 2.5 %) and 4 curing ages (1-day, 3-days, 7-days and 28-days curing systems). By discussing the microscopic morphology, hydration products and pore changes of LC3-ECCs, the development law of its compressive strength and flexural strength was explained. Both C2 and PPFs are not conducive to the fluidity of the matrix. The increase of fiber content will result in the decreasing of 28-days compressive strength of LC3-ECCs, which is from 57.1 M to 44.2 MPa. The increasing of fiber dosage will lead to the rising of 28-days flexural strength of LC3-ECCs, which is from 4.8 MPa to 7.7 MPa. The PP fiber and the LC3 matrix can be effectively bonded together. During the hydration process from 1 d to 28 d, the portlandite in the LC3 system decreases from 3.2 % to 2.2 %. In contrast, the bound water increases from 7.7 % to 11.5 %. It can reflect the degree of hydration of the LC3 system. The utilization of PP fibers will increase the pore size of 0.2 μm in the LC3 system, thereby reducing the mechanical behavior of LC3-ECC.

As the eco-friendly ECCs incorporating low-carbon LC3, PP-ECCs can be applied to structural components to explore its more applications. In the future, it is possible to design ECCs incorporating different solid waste materials and low-carbon LC3, and explore the performance development of this eco-efficient ECCs in different degraded environments.

Declaration of Competing Interest

The authors declare that they have no known competing financial interests or personal relationships that could have appeared to influence the work reported in this paper.

Data Availability

Data will be made available on request.

Acknowledgements

The work described in this paper was fully supported by grants Shenzhen Sustainable Development Technology Project (2021N031), Shenzhen International Cooperation Research Project (GJHZ20180928155602083) and Guangdong Provincial Key Laboratory of Durability for Marine Civil Engineering (2020B1212060074).

References

[1] Y.C. Díaz, S.S. Berriel, U. Heierli, A.R. Favier, I.R.S. Machado, K.L. Scrivener, et al., Limestone calcined clay cement as a low-carbon solution to meet expanding cement demand in emerging economies, Dev. Eng. 2 (2017) 82–91.
[2] K.L. Scrivener, Options for the future of cement, Indian Concr. J. 88 (7) (2014) 11–21.
[3] M.S. Imbabi, C. Carrigan, S. McKenna, Trends and developments in green cement and concrete technology, Int. J. Sustain. Built Environ. 1 (2) (2012) 194–216.
[4] L.K. Turner, F.G. Collins, Carbon dioxide equivalent (CO2-e) emissions: a comparison between geopolymer and OPC cement concrete, Constr. Build. Mater. 43 (2013) 125–130.
[5] M. Schneider, M. Romer, M. Tschudin, H. Bolio, Sustainable cement production—present and future, Cem. Concr. Res. 41 (7) (2011) 642–650.
[6] M.C.G. Juenger, F. Winnefeld, J.L. Provis, J.H. Ideker, Advances in alternative cementitious binders, Cem. Concr. Res. 41 (12) (2011) 1232–1243.
[7] B. Lothenbach, K. Scrivener, R.D. Hooton, Supplementary cementitious materials, Cem. Concr. Res. 41 (12) (2011) 1244–1256.
[8] E. Crossin, The greenhouse gas implications of using ground granulated blast furnace slag as a cement substitute, J. Clean. Prod. 95 (2015) 101–108.
[9] R. Siddique, Utilization of silica fume in concrete: review of hardened properties, Resour. Conserv. Recycl. 55 (11) (2011) 923–932.
[10] E. Özbay, M. Erdemir, H.İ. Durmuş, Utilization and efficiency of ground granulated blast furnace slag on concrete properties – a review, Constr. Build. Mater. 105 (2016) 423–434.
[11] A.K. Saha, M.N.N. Khan, P.K. Sarker, F.A. Shaikh, A. Pramanik, The ASR mechanism of reactive aggregates in concrete and its mitigation by fly ash: a critical review, Constr. Build. Mater. 171 (2018) 743–758.
[12] Y. Liu, T.-C. Ling, Potential use of calcined kaolinite-based wastes as cement replacements in concrete – an overview, IOP Conf. Ser.: Mater. Sci. Eng. 431 (3) (2018), 032006.
[13] M.C.G. Juenger, R. Siddique, Recent advances in understanding the role of supplementary cementitious materials in concrete, Cem. Concr. Res. 78 (2015) 71–80.
[14] D.P. Bentz, Powder additions to mitigate retardation in high-volume fly ash mixtures, Mater. J. 107 (5) (2010) 508–514.
[15] A.C. Emmanuel, P. Haldar, S. Maity, S. Bishnoi, Second pilot production of limestone calcined clay cement in India: the experience, Indian Concr. J. 90 (2016) 57–63.
[16] S.S. Berriel, A. Favier, E.R. Domínguez, I.R.S. Machado, U. Heierli, K. Scrivener, et al., Assessing the environmental and economic potential of limestone calcined clay cement in Cuba, J. Clean. Prod. 124 (2016) 361–369.
[17] K. Scrivener, A. Favier, Calcined Clays for Sustainable Concrete, Springer, 2015.
[18] S. Krishnan, Industrial production of limestone calcined clay cement: experience and insights, Green Mater. 7 (1) (2018) 15–27.
[19] M.T. Ronald, H. Pengkun, K. Shiho, S. Tongbo, C. Xin, The role of limestone and calcined clay on the rheological properties of LC3, Cem. Concr. Compos. 107 (2020), 103516.
[20] Y. Dhandapani, T. Sakthivel, M. Santhanam, R. Gettu, R.G. Pillai, Mechanical properties and durability performance of concretes with limestone calcined clay cement (LC 3), Cem. Concr. Res. 107 (2018) 136–151.
[21] F. Avet, K. Scrivener, Investigation of the calcined kaolinite content on the hydration of limestone calcined clay cement (LC 3), Cem. Concr. Res. 107 (2018) 124–135.
[22] V.C. Li, From micromechanics to structural engineering-the design of cementitous composites for civil engineering applications, Struct. Eng./Earthq. Eng. 10 (2) (1993) 37–48.
[23] V.C. Li, Advances in ECC research, in: Concrete: Material Science to Application. Engineered Materials 206, 2002, pp. 373–400.
[24] Z. He, Y. Kequan, C. LV, Sprayable engineered cementitious composites (ECC) using calcined clay limestone cement (LC3) and PP fiber, Cem. Concr. Compos. 115 (2021), 103868.
[25] Z. He, Z. Duo, W. Tianyu, W. Haoliang C.L.V., Mechanical and self-healing behavior of low carbon engineered cementitious composites reinforced with PP-fibers, Constr. Build. Mater. 259 (2020), 119805.
[26] GAQSIQ, Method of testing cements-Determination of strength (ISO Method), GB/T 17671-1999, National Standards of the People's Republic of China (in Chinese), 1999.
[27] S.A. GAQSIQ, Test method for fluidity of cement mortar, GB/T2419-2005, National Standards of the People's Republic of China (in Chinese), 2005.
[28] S.A. GAQSIQ, Common Portland Cement, GB 175-2007, National Standards of the People's Republic of China (in Chinese), 2007.
[29] Y. Jing, W.H. Liang, K.M.D, L. Gengying, L.C. KY, Compressive strength and environmental impact of sustainable blended cement with high-dosage limestone and calcined clay (LC2), J. Clean. Prod. 278 (2021), 123616.
[30] K. Scrivener, Impacting factors and properties of limestone calcined clay cements (LC3), Green Mater. 7 (1) (2018) 3–14.
[31] S. Ferreiro, D. Herfort, J.S. Damtoft, Effect of raw clay type, fineness, water-to-cement ratio and fly ash addition on workability and strength performance of calcined clay – limestone Portland cements, Cem. Concr. Res. 101 (2017) 1–12.
[32] F.N. Santos, S.R.G.d. Sousa, A.J.F. Bombard, S.L. Vieira, Rheological study of cement paste with metakaolin and/or limestone filler using mixture design of experiments, Constr. Build. Mater. 143 (2017) 92–103.
[33] E.-H. Yang, S. Wang, Y. Yang, V.C. Li, Fiber-bridging constitutive law of engineered cementitious composites, J. Adv. Concr. Technol. 6 (1) (2008) 181–193.
[34] A. AG, N. Hassan, M.H.M, R. Tyson, D. Nirmal, Feasibility of low fiber content PVA-ECC for jointless pavement application, Constr. Build. Mater. 268 (2021), 121131.
[35] Y. Ding, J.-P. Liu, Y.-L. Bai, Linkage of multi-scale performances of nano-CaCO 3 modified ultra-high performance engineered cementitious composites (UHP-ECC), Constr. Build. Mater. 234 (2020), 117418.
[36] A.K. Tiwari, S. Chowdhury, Relative evaluation of performance of limestone calcined clay cement compared with Portland pozzolana cement, J. Asian Concr. Fed. 2 (2) (2016) 110–116.
[37] F. Avet, E. Boehm-Courjault, K. Scrivener, Investigation of C-A-S-H composition, morphology and density in limestone calcined clay cement (LC 3), Cem. Concr. Res. 115 (2019) 70–79.
[38] W. Kunther, Z. Dai, J. Skibsted, Thermodynamic modeling of hydrated white Portland cement–metakaolin–limestone blends utilizing hydration kinetics from 29Si MAS NMR spectroscopy, Cem. Concr. Res. 86 (2016) 29–41.
[39] S. Krishnan, S. Bishnoi, A numerical approach for designing composite cements with calcined clay and limestone, Cem. Concr. Res. 138 (2020), 106232.
[40] T. Matschei, B. Lothenbach, F.P. Glasser, The AFm phase in Portland cement, Cem. Concr. Res. 37 (2) (2006) 118–130.

[41] M.U. Okoronkwo, F.P. Glasser, Compatibility of hydrogarnet, Ca3Al2(SiO4)x(OH)4(3−x), with sulfate and carbonate-bearing cement phases: 5–85 °C, Cem. Concr. Res. 83 (2016) 86–96.
[42] T. Matschei, B. Lothenbach, F.P. Glasser, The role of calcium carbonate in cement hydration, Cem. Concr. Res. 37 (4) (2007) 551–558.
[43] D. Zhang, B. Jaworska, H. Zhu, K. Dahlquist, V.C. Li, Engineered cementitious composites (ECC) with limestone calcined clay cement (LC 3), Cem. Concr. Compos. 114 (2020), 103766.
[44] M. Şahmaran, E. Özbay, H.E. Yücel, M. Lachemi, V.C. Li, Effect of fly ash and PVA fiber on microstructural damage and residual properties of engineered cementitious composites exposed to high temperatures, J. Mater. Civ. Eng. 23 (12) (2011) 1735–1745.
[45] D. Zhang, Y. Shao, Surface scaling of CO2-cured concrete exposed to freeze-thaw cycles, J. CO2 Util. 27 (2018) 137–144.
[46] P. Monteiro, Concrete: Microstructure, Properties, and Materials, McGraw-Hill Publishing, 2006.
[47] E.-H. Yang, Y. Yang, V.C. Li, Use of high volumes of fly ash to improve ECC mechanical properties and material greenness, Mater. J. 104 (6) (2007) 620–628.
[48] J. Yu, C. Lu, C.K.Y. Leung, G. Li, Mechanical properties of green structural concrete with ultrahigh-volume fly ash, Constr. Build. Mater. 147 (2017) 510–518.
[49] J. Yu, Y. Chen, C.K.Y. Leung, Mechanical performance of strain-hardening cementitious composites (SHCC) with hybrid polyvinyl alcohol and steel fibers, Compos. Struct. 226 (2019), 111198.
[50] J. Yu, H.-L. Wu, C.K.Y. Leung, Feasibility of using ultrahigh-volume limestone-calcined clay blend to develop sustainable medium-strength engineered cementitious composites (ECC), J. Clean. Prod. 262 (2020), 121343.
[51] D. Zhang, J. Yu, H. Wu, B. Jaworska, B.R. Ellis, V.C. Li, Discontinuous micro-fibers as intrinsic reinforcement for ductile engineered cementitious composites (ECC), Compos. Part B 184 (2020), 107741.
[52] Y.S. Song, J.R. Youn, T.G. Gutowski, Life cycle energy analysis of fiber-reinforced composites, Compos. Part A 40 (8) (2009) 1257–1265.
[53] R. Gettu, A. Patel, V. Rathi, S. Prakasan, A.S. Basavaraj, S. Palaniappan, et al., Influence of supplementary cementitious materials on the sustainability parameters of cements and concretes in the Indian context, Mater. Struct. 52 (1) (2019) 1–11.
[54] G. Hammond, C. Jones, Inventory of Carbon and Energy', University of Bath, 2008.
[55] K. Tosun-Felekoğlu, E. Gödek, M. Keskinateş, B. Felekoğlu, Utilization and selection of proper fly ash in cost effective green HTPP-ECC design, J. Clean. Prod. 149 (2017) 557–568.
[56] B. Felekoglu, K. Tosun-Felekoglu, R. Ranade, Q. Zhang, V.C. Li, Influence of matrix flowability, fiber mixing procedure, and curing conditions on the mechanical performance of HTPP-ECC, Compos. Part B 60 (2014) 359–370.